

¹ Regional Climate Simulations with the Community ² Earth System Model

A. Gettelman¹, P. Callaghan¹, V. E. Larson², C. M. Zarzycki¹, J.

Bacmeister¹, P. H. Lauritzen¹, P. A. Bogenschutz^{1,3} and R. Neale¹

¹National Center for Atmospheric
Research, Boulder, CO, USA.

²University of Wisconsin — Milwaukee,
Milwaukee, WI, USA

³Lawrence Livermore National
Laboratory, Livermore, CA, USA

3 **Abstract.** The Spectral Element (SE) Variable Resolution (VR) mesh
4 dynamical core is tested in developmental versions of the Community Earth
5 System Model version 2 (CESM2). The SE dynamical core is tested in ide-
6 alized, aquaplanet and full-physics configurations to evaluate variable-resolution
7 simulations against uniform high and uniform low resolution simulations. Dif-
8 ferent physical parameterization suites are also evaluated to gauge their sen-
9 sitivity to resolution. Idealized variable-resolution cases compare well to high
10 resolution tests. More recent versions of the atmospheric physics, including
11 cloud schemes for CESM2, are less sensitive to changes in horizontal reso-
12 lution. Most of the sensitivity is due to sensitivity to time step and inter-
13 actions between deep convection and large scale condensation, which is ex-
14 pected from the closure methods. The resulting full physics SE-VR model
15 produces a similar climate to the global low resolution mesh and similar high
16 frequency statistics in the high resolution region. The SE-VR simulations are
17 able to reproduce uniform high resolution results, making them an effective
18 tool for regional climate simulations at lower computational cost. Some bi-
19 ases are reduced (orographic precipitation in Western United States), but
20 biases do not necessarily go away at high resolution (e.g. summertime sur-
21 face temperatures). Variable-resolution grids are a viable alternative to tra-
22 ditional nesting for regional climate studies and are available in CESM2.

1. Introduction

23 A significant goal of climate simulation is to understand possible impacts of climate
24 change. No one is killed by the global average mean temperature, rather, many impacts
25 of climate change occur on small scales: such as the scale of a watershed or the synoptic
26 scale of a squall line. Few climate models can resolve these scales, which are on the order
27 of 25km (0.25°) or less.

28 Recently however, high resolution simulations have become available due to advances in
29 computational power. In uniform high resolution configurations, the Community Atmo-
30 sphere Model (CAM) version 5 [Neale *et al.*, 2010] has been run to look at high frequency
31 climate statistics [Wehner *et al.*, 2014; Bacmeister *et al.*, 2014], including tropical cyclones
32 [Bacmeister *et al.*, 2016], and has also been run coupled to an ocean to look at long term
33 climate change [Small *et al.*, 2014].

34 The computational cost of a 0.25° global grid is significant on current high performance
35 computing platforms for long-duration simulations. So ‘regional climate models’ have
36 been developed using typically mesoscale models over limited regions of the planet, to
37 try to reproduce higher frequency statistics for smaller regions of the globe. These are
38 described in reviews by McGregor [1997], Laprise [2008], Mearns *et al.* [2012] (for regional
39 simulations over the United States), and many others too numerous to list in detail.
40 However, these models must be driven at the boundaries, generally by output from a
41 different lower resolution global model. This may create significant inconsistencies [Ringer
42 *et al.*, 2011].

43 Several studies have begun to investigate another approach to regional climate simu-
44 lation that uses global models with static variable-resolution (VR) meshes, in which the
45 horizontal size of a grid box changes. These include investigating climate aspects such
46 as tropical cyclones [*Zarzycki and Jablonowski, 2014, 2015*], orographic forcing [*Zarzycki*
47 *et al., 2015; Rhoades et al., 2016; Wu et al., 2017*], and regional precipitation patterns
48 [*Rauscher et al., 2012; Harris and Lin, 2013; Sakaguchi et al., 2015; Huang et al., 2016*].

49 This work presents simulations that use the Spectral Element (SE) dynamical core
50 [*Taylor, 2011, and references herein*] with variable resolution (VR) in the Community
51 Earth System Model version 2 (CESM2), specifically in the atmospheric component, the
52 Community Atmosphere Model (CAM). The implementation of the SE dynamical core
53 in CAM and the adjustments for CAM6 are described by P. Lauritzen et al (NCAR
54 CESM2.0 release of CAM-SE: A reformulation of the spectral-element dynamical core in
55 dry-mass vertical coordinates with comprehensive treatment of condensates and energy, to
56 be submitted to JAMES, 2017). Different versions of the CAM physical parameterizations
57 are tested as well. The goal is to evaluate the dynamics and the physical parameterizations
58 of the model with different resolutions and with variable resolution.

59 This is a test of what is commonly called ‘scale aware’ parameterizations. Scale aware
60 implies the parameterization knows the length scale, which is not true for most physical
61 parameterizations in GCMs. We prefer to state that we are seeking ‘scale insensitive’
62 parameterizations, that at a minimum are robust across uniform resolutions and changes
63 in resolution. Ultimately we would like the solutions to converge as we refine in the
64 horizontal, vertical and in time. Our study differs from previous work in that it seeks
65 to benchmark VR climate statistics against uniform versions of the same model, and to

66 document the variable resolution version of the atmosphere for CESM2 and the scale-
67 sensitivity of its physical parameterizations.

68 This study will first explore the dynamics using idealized simulations, then explore dif-
69 ferent versions of the CAM physics with aquaplanet simulations. Finally, we will analyze
70 'full physics' simulations of the latest version of CAM. We will look at both global and
71 local statistics, and in particular statistics of extreme events. This includes mean cli-
72 mate metrics for surface temperature (T_s) and precipitation as well as the variability of
73 precipitation (intensity, diurnal cycle) and extremes of temperature.

74 The focus is on evaluation of VR grids in CESM2 relative to configurations with uniform
75 high resolution. Can the same climate statistics be achieved at lower cost for metrics that
76 matter by using regional refinement? The central hypothesis of this work is to show that
77 CAM-SE-VR and CESM2 configurations can successfully match uniform high resolution
78 statistics and be used for consistent regional climate simulations.

79 Section 2 contains a description of the hierarchy of models used in this study. Results
80 are in Section 3 and a summary and conclusions is contained in Section 4.

2. Methodology

81 This section describes the model simulations used in the study. The philosophy follows
82 the evolution of the VR model. First tests are conducted with idealized test cases for
83 mid-latitude baroclinic instability. Then aquaplanet simulations are conducted to look
84 at full physics results, first with a refined mesh in the extratropics over a section of
85 longitudes (identical to the idealized case), and then with a refined mesh in a particular
86 longitude region in the tropics. The aquaplanet tests are done with several versions of
87 the atmospheric model physics as described below. Finally, full physics simulations using

88 a physics suite similar to the final CAM6 physics are conducted with topography and a
89 refined mesh over the Continental United States (CONUS).

90 The model is a developmental version of CAM, the atmospheric component of CESM.
91 The code base contains developmental code for features to be released in CESM2. The
92 atmosphere model uses the Spectral Element (SE) dynamical core [Taylor, 2011], with
93 the variable-resolution (VR) configuration described in Zarzycki *et al.* [2014a]. Physi-
94 cal parameterizations include several versions of the atmosphere model. CAM4 [Neale
95 *et al.*, 2013] is the atmosphere model for CCSM4 [Gent *et al.*, 2011], CAM5 [Neale *et al.*,
96 2010] is the atmosphere model for CESM1 [Hurrell *et al.*, 2013]. We also use a version
97 of the atmosphere model CAM5 that includes a new unified moist turbulence parameter-
98 ization, Cloud Layers Unified by Binormals (CLUBB), developed by Golaz *et al.* [2002]
99 and Larson *et al.* [2002] and implemented in CAM by Bogenschutz *et al.* [2013], called
100 CAM5-CLUBB. Finally we use a version that contains CLUBB plus updated aerosols
101 and cloud microphysics (MG2) described by Gettelman [2015]. We call this last version
102 CAM6 α .

103 A series of resolutions were tested, corresponding to a uniform low resolution of $\sim 1^\circ$
104 (100km) on a cubed sphere. This has 30x30 elements per cube face and each element has
105 4 quadrature points in each coordinate direction with duplicate points on the boundaries
106 and is called ‘ne30’. Uniform high resolution has 120x120 elements per face (correspond-
107 ing to $\sim 0.25^\circ$ or 25km horizontal resolution), and is called ‘ne120’. The variable mesh
108 simulations have ne120 resolution in the refined region, and adjust smoothly to ne30 out-
109 side of it. A grid with regional refinement over the Continental United States (CONUS)
110 is shown in Figure 1.

2.1. Idealized Physics

111 Idealized physics test cases were designed to analyze the dynamics of the spectral ele-
112 ment dynamical core using the baroclinic wave test case of *Jablonowski and Williamson*
113 [2006]. The baroclinic wave test with idealized physics on an aquaplanet was run with (A)
114 uniform high resolution (0.25° , ne120 in the SE nomenclature), (B) uniform low resolution
115 (1° , ne30) and (C) a VR case with a high-resolution region was placed from $25\text{--}65^\circ\text{N}$ over
116 60° of longitude. Simulations were run for 30 days.

117 Idealized physics simulations were used to test the internal damping in the SE core.
118 The SE dynamical core uses a resolution dependent setting for the fourth-order horizontal
119 hyperviscosity operator (ν) to damp waves that are not resolvable [*Zarzycki et al.*, 2014a].
120 Different values of hyperviscosity were tested. (1) The standard VR case (VRhVR), ν
121 ranges from 1×10^{13} at 0.25° to 1×10^{15} at 1° , (2) a VR case with a non-scale-selective
122 hyperviscosity appropriate for the ne30 low resolution case (VRh30, constant $\nu = 1 \times$
123 10^{15}) and (3) a low resolution (ne30) case with hyperviscosity option set to the variable-
124 resolution settings (ne30hVR, ν approximately 1×10^{13}).

2.2. Aquaplanet

125 Next, simulations were performed using the full physical parameterization suite for
126 the atmosphere, but with a uniform ‘aquaplanet’ land surface. These simulations place a
127 variable mesh (a) in the midlatitudes from $25\text{--}65^\circ\text{N}$ as with the idealized test case, and (b)
128 with a tropical mesh from 30°S to 30°N and over 60° of longitude. These simulations were
129 designed to test physical parameterization suites and were performed with CAM4, CAM5
130 and CAM5-CLUBB physical parameterizations. Note that CLUBB actually knows the
131 grid box size and uses this information to truncate the turbulent length scale. Simulations

132 were run for 3 years under uniform equinox conditions. The high resolution portion of
133 the next is at 0.25° (ne120) with the low resolution portion at 1° (ne30). ν ranges from
134 1×10^{13} in the high-resolution region to 1×10^{15} in the low-resolution domain. The physics
135 timestep is 900s.

2.3. Full Physics Simulations

136 Finally, full physics simulations were run with the CAM6 α configuration, including all
137 the physical parameterizations for CAM6. Simulations were run with uniform ne120 (High
138 Resolution, 0.25° , $\sim 25\text{km}$), and uniform ne30 (Low Resolution, 1° , $\sim 100\text{km}$). Simulations
139 were run for 26 years from 1980–2005. The VR mesh has high resolution from 22.5°N
140 to 50°N and 230° to 295° longitude (130°W to 65°W), illustrated in Figure 1. We use a
141 timestep of 900s for all simulations (typically a low resolution CAM6 simulation would
142 use 1800s), and a coupling frequency between the microphysics and CLUBB of 300s (3
143 couplings per timestep), following *Gettelman and Morrison* [2015]. The only modification
144 between the simulations, is that to keep the energy more in balance we adjust the critical
145 diameter for ice autoconversion (DCS) in the high resolution (ne120) simulation only
146 (increase DCS from 140 to 275 microns). This increases high cirrus clouds, compensating
147 for slightly reduced deep convective activity. The hyperviscosity coefficient is set to $\nu =$
148 1×10^{15} in the ne30 simulation, $\nu = 1 \times 10^{13}$ in the ne120 simulation, and correspondingly
149 scaled as a function of grid size using these base coefficients in the VR run as described
150 for the idealized cases above.

2.4. Observational Comparisons

151 For comparison to observations with the full physics simulations, we use several different
152 data sets. For climatological comparisons, we use the European Center Interim Reanalysis
153 (ERA-Interim) at ~ 70 km resolution [Dee *et al.*, 2011]. For analysis of the diurnal cycle of
154 precipitation we use precipitation data from the Tropical Rainfall Measuring Mission
155 (TRMM) [Kummerow *et al.*, 1998] based on TRMM 3B42 0.25° 3 hourly gridded data.

156 The National Oceanic and Atmospheric Administration (NOAA) Climate Prediction
157 Center (CPC) provides analysis of daily precipitation for the Continental United States
158 at 0.25° by combining rain gauge data with an optimal interpolation objective analysis
159 technique [Chen *et al.*, 2008].

160 Finally we also use precipitation and surface temperature daily and 3 hourly from
161 the North American Regional Reanalysis (NARR). NARR is a high resolution (32km,
162 3-hourly) reanalysis product dynamically downscaled over N. America [Mesinger *et al.*,
163 2006].

164 All data are concurrent in time with model simulations (1980-2005). Full physics and
165 terrain model simulations follow the protocol for Atmospheric Model Intercomparison
166 Project (AMIP) simulations with monthly mean observed ocean temperature and aerosol
167 and trace gas emissions from 1979-2005 as boundary forcing. The first year is not analyzed.
168 Land temperatures are prognostic. As a result, high frequency variability in the model
169 simulations will not correspond to any particularly observed weather event.

3. Results

3.1. Idealized test case: Dry baroclinic wave

170 Figure 2 illustrates the level 2 (L2) Error Norms for various configurations using the
171 uniform resolution 0.25° (ne120) case as the reference. L2 error norms are a root-mean-
172 square error approach to evaluate symmetry deviations from the zonal average. L2 Error
173 Norms are defined as in *Jablonowski and Williamson* [2006].

174 The key feature is that out to 8 days or so the variable mesh simulation with appropriate
175 damping (setting the hyperviscosity for variable mesh settings, VRhVR) has low L2 Error
176 scores inside the region of refinement (low error norm relative to the reference uniform
177 ne120 high resolution) compared to other cases. This shows regional refinement maintains
178 fine-scale structure of features and is also good performance relative to other dynamical
179 cores discussed in *Jablonowski and Williamson* [2006]. When the hyperviscosity is set
180 to the globally-uniform low resolution coefficient (VRh30), results are not as satisfactory,
181 implying that the additional explicit diffusion is damping any improved resolvable scales
182 in the high-resolution nest. Setting the hyperviscosity in an ne30 case to the variable-
183 resolution settings (ne30hVR) produces a very similar result to uniform low resolution,
184 which is expected since the variable-resolution hyperviscosity scaling in *Zarzycki et al.*
185 [2014a] is designed to match the uniform configuration when unrefined grids are utilized
186 within the variable-resolution framework. This also further confirms appropriate behavior
187 of the scaling mechanism used for variable-resolution runs when compared to standard
188 uniform resolution configurations. Error norms for all configurations eventually all con-
189 verge to similar values in agreement with *Ringler et al.* [2011], who found that analytic
190 errors are eventually constrained by the lowest resolution of a variable-resolution mesh,
191 not the refined patch.

192 Figure 2 illustrates that the variable mesh correctly represents the dynamics when at the
193 same resolution of a uniform high-resolution grid, consistent with the findings in *Zarzycki*
194 *et al.* [2014b]. Evaluation of temperature perturbations (not shown) indicates that VR
195 simulations in the low resolution region in mid-latitudes downstream of the breaking wave
196 look more like the high resolution simulation. Thus once waves are generated in the high-
197 resolution region, they propagate as expected into and through the low resolution region.
198 Scales which are not resolvable in the low resolution are damped as they enter the low
199 resolution region via the resolution-aware hyperviscosity operator but already-resolved
200 scales generated in the high-resolution nest are allowed to affect the mean flow, even in
201 the low-resolution region.

3.2. Aquaplanet simulations

202 3.2.1. Mid Latitude Refinement

203 Results of the idealized test case simulations provide initial confidence in the configu-
204 ration and in the dynamical core. The next step is to run the aquaplanet model with full
205 physics. This was done for the mid-latitude refinement case again. Three different physics
206 packages were used: CAM4, CAM5 and CAM5-CLUBB. The CAM5-CLUBB configura-
207 tion is an intermediate between CAM5 and CAM6, with the important addition of the
208 CLUBB unified turbulence scheme. Note that all three configurations use the same ba-
209 sic deep convective scheme (*Zhang and McFarlane* [1995], hereafter ZM), with a slightly
210 different closure in CAM5 and CAM5-CLUBB [*Neale et al.*, 2008]. But the shallow convec-
211 tive scheme is different in all three: *Hack* [1994] for CAM4, *Park and Bretherton* [2009] for
212 CAM5 and CLUBB [*Bogenschutz et al.*, 2010, 2013] for CAM5-CLUBB. Note that CLUBB

213 combines the macrophysics (cloud fraction and large scale condensation), boundary layer
214 and shallow convection into one scheme that drives stratiform microphysics.

215 Figure 3 illustrates means in the 25°N–60°N latitude band for zonal mean (Blue), in-
216 side the refined region (Green) and outside (Red). Different resolutions (Ne30,Ne120,Var)
217 are shown at different x-axis positions. Each of the 3 physics suites is denoted by a
218 uniquely shaped line marker: CAM4 (square), CAM5 (circle) and CAM5-CLUBB (trian-
219 gle). Figure 3A illustrates mean cloud fraction. CAM4 (squares) in the variable resolution
220 configuration (Var) has a large difference in cloud fraction between the region inside and
221 outside of the mesh. The error bars represent one standard deviation (σ) of aquaplanet
222 monthly means in a region the size of the variable mesh region and are similar for all
223 simulations ($\sigma \sim 0.02$ for cloud fraction). Differences inside and outside of the high res-
224 olution region in uniform cases are indicative of variability of the physics with scales.
225 CAM4 also has a big difference in cloud fraction (Figure 3A) between Ne120 (high res)
226 or variable mesh at about 0.57 and Ne30 (about 0.67). Thus CAM4 VR inside the mesh
227 (Var, Green) looks like the high resolution (ne120) CAM4 while outside the mesh (Red)
228 and zonal mean (Blue) look like the low resolution (Ne30) CAM4. This indicates the
229 cloud fraction is dependent on resolution in CAM4. CAM5 (circle) and CAM-CLUBB
230 (triangle) have more similar mean cloud fractions inside and outside of the mesh in all
231 cases, and similar results across resolutions.

232 Figure 3B indicates a similar result for 850hPa zonal wind speed. The CAM4 solutions
233 vary by almost 3ms^{-1} between ne30 and ne120. The standard deviation is about 2ms^{-1} so
234 it is not clear that these differences are significant. Interestingly the VR simulation looks
235 like the low resolution. There is slightly more variation across resolution in zonal wind for

236 CAM5 and CAM5-CLUBB configurations. Figure 3C illustrates results for longwave (LW)
237 cloud radiative effects (CRE). The standard deviation is about 2 Wm^{-2} In CAM4 (square),
238 cloud forcing differs by 5 Wm^{-2} (20%) inside and outside of the variable mesh region, and
239 also between resolutions. This is similar to cloud fraction (Figure 3A), since the two fields
240 are related. CAM5 (circle) varies by 2 Wm^{-2} and CAM5-CLUBB (triangle) by 0.5 Wm^{-2}
241 across resolutions (less than the variability), and the VR simulation tends to look more
242 like the high resolution for CAM5 and CAM5-CLUBB. There is little difference inside and
243 outside of the high resolution region for CAM5 and CAM5-CLUBB. Finally, Figure 3D
244 illustrates similar results for shortwave cloud radiative effects (SWCRE). The standard
245 deviation is about 4 Wm^{-2} . There is more variation in SWCRE across resolutions in all
246 the configurations, but for CAM5-CLUBB and CAM4, the VR simulation is closer to the
247 high resolution, and results are similar inside and outside of the VR region for CAM5 and
248 CAM5-CLUBB.

249 In general, CAM5 and CAM5-CLUBB are quite stable in mid-latitude cloud systems,
250 and vary little in any single run inside or outside of the high resolution region. CAM4 how-
251 ever has a strong resolution dependence, consistent with previous findings [*Williamson,*
252 *2008; Rauscher et al., 2012; Zarzycki et al., 2014a*].

253 **3.2.2. Tropical Refinement**

254 Experiments have been conducted with a refined mesh region in the tropics, again
255 using an aquaplanet configuration. The mesh is centered on the equator and extends 60°
256 of longitude and from 30°S to 30°N latitude. This is indicated as the red lines on Figure 4.

257 Figure 4 presents a map of the mean tropical precipitation rate from these variable
258 mesh simulations. CAM4 (Figure 4C) has high precipitation in the refined region over

259 the equatorial intertropical convergence zone, CAM5 (Figure 4B) has less precipitation in
260 the high-resolution region and is more uniform, and CAM5-CLUBB (Figure 4A) has high
261 precipitation both inside and outside of the high-resolution region. The total precipitation
262 (PRECT) is more similar inside and outside the high-resolution region along the equator
263 in CAM5-CLUBB (Figure 4A) than in the other configurations (Figure 4B,C).

264 Figure 5 illustrates that in all three simulations, as expected, the ratio of large scale
265 (PRECL: Figure 5A-C) to convective (PRECC: Figure 5D-F) precipitation is greater
266 inside the high-resolution region than in the outer, low-resolution region. The time step is
267 the same in both regions, so the convective relaxation time in relation to the time step is
268 the same. But the vertical velocity forcing supersaturation for the large scale condensation
269 is likely to be higher in the high resolution region, driving more condensation. Since the
270 condensation in the macrophysics is generally not limited with a timescale, it removes
271 water right away. This would increase stratiform precipitation in the refined regions, as
272 seen in all cases in Figure 5. And more condensation done by the stratiform scheme with
273 fixed precipitable water means less available for convection.

274 The compensation between convective (PRECC) and large scale (PRECL) precipitation
275 occurs in all three schemes, but in CAM5-CLUBB (Figure 5A,D) and CAM5 (Figure 5B,E)
276 there is less variation in total precipitation inside and outside of the high resolution
277 region than in CAM4 (Figure 5C,F). This is an important property since VR aquaplanet
278 configurations where total precipitation varies greatly between high- and low-resolution
279 regions can drive spurious Gill-type circulations associated with asymmetric latent heating
280 as a function of longitude [*Rauscher et al.*, 2012; *Zarzycki et al.*, 2014a].

281 Finally we show sets of vertical profiles of the different physics tendency terms averaged
282 5°S to 5°N inside (solid lines) and outside (dashed lines) of the high resolution region.
283 Figure 6 shows temperature (T) and Figure 7 illustrates specific humidity (Q) tenden-
284 cies. The different terms are for the total physics tendency (Black: DTCOND and DCQ
285 for temperature and humidity respectively), the macro and microphysics (Blue: MPDT
286 and MPDQ, this includes all condensation from CLUBB), the shallow convection (Red:
287 CMFDT and CMFDQ: note that CLUBB does not have any separate shallow convec-
288 tion and so the red lines are zero and their contributions are included in MPDT and
289 MPDQ) and tendencies for the deep convection (Green: ZMDT and ZMDQ). Note that
290 the budgets will not totally balance due to diffusion and other small terms.

291 The temperature tendencies in Figure 6 indicate similar results to the mean tropical
292 precipitation figures (Figure 4 and Figure 5). There is a difference in deep convective
293 (green) and large scale (blue) precipitation inside (solid) and outside (dashed) of the high
294 resolution region. This occurs in most of the simulations, with shallow convection differing
295 the most in CAM4 (Figure 6C). Note that the CAM5-CLUBB simulation (Figure 6A)
296 has more constant total tendencies inside and outside of the high resolution region than
297 the other two configurations for stratiform microphysics and CLUBB. The ZM humidity
298 tendency does change, and it is balanced by a change in mixing (not shown in the moist
299 physics tendencies).

300 The humidity tendencies are shown in Figure 7. CAM5-CLUBB (Figure 7A) has more
301 similar humidity tendencies inside and outside of the refined region (solid and dashed black
302 lines) than does CAM5 or CAM4. CAM5 (Figure 7B) has very different performance (es-
303 pecially of the microphysics, blue), and note that the microphysics/macrophysics (MPDQ)

304 and shallow convection (CMFDQ) are operating in opposition to each other: shallow con-
305 vection seems to remove condensate that microphysics puts back. This may be a result
306 of the coupling of the shallow convective detrainment in CAM5. Also note that CAM5-
307 CLUBB has its main tendency for low clouds higher (800hPa) than CAM4 or CAM5
308 (950hPa).

3.3. Climate Simulations

309 We now move on to full climate simulations that include topography and an active land
310 surface. We focus on the CAM5-CLUBB physics, and upgrade the physical parameteri-
311 zations in addition to CLUBB to use versions that are part of CAM6 (new ice nucleation,
312 new cloud microphysics, and modified aerosol model). This model formulation is a prelim-
313 inary version of CAM6, (called CAM6 α) using the land component CLM4 from CESM1.
314 There are slightly different tuning parameters than the final version of CAM6, but the
315 basic physics is the same, except for a new surface drag scheme which was not available.
316 We focus now on a variable mesh over the Continental United States (CONUS) illustrated
317 in Figure 1, and described in Section 2.

318 Globally the three simulations have very similar climates. An analysis indicates however
319 that the low resolution (ne30) and VR simulations perform slightly better against obser-
320 vations than the high resolution (ne120) simulation. For example, the RMSE for annual
321 precipitation rate against Global Precipitation Climatology Project (GPCP) rain rates is
322 0.93 mm day⁻¹ for uniform ne30, 0.95 mm day⁻¹ for VR but 1.12 mm day⁻¹ for uniform
323 ne120. This is also indicated by an overall multivariate skill score following *Taylor* [2001],
324 including precipitation, cloud radiative effects, surface stress and temperature, and free
325 tropospheric zonal wind. This is likely because CAM6 α was developed and optimized

326 at low resolution, and there are some differences with resolution (as noted above). This
327 global optimization or tuning affects results below.

328 First we assess the stability of seasonal means for important quantities in the variable
329 mesh region. We analyze climatological biases relative to observations, to see if there
330 are regional or coherent differences between simulations. We compare the simulations to
331 a common metric. For climatological data, we use European Center Interim Reanalysis
332 (ERA-Interim) surface temperature (Ts) and precipitation data, averaged over the same 1980-
333 2005 period. Data is gridded to $1^\circ \times 1^\circ$ for all simulations and ERA-Interim before comparison.
334 Figure 8 illustrates the percent difference between the CAM6 α CONUS simulations and
335 ERA-Interim climatological precipitation means for summer (June–August). Over land, summer
336 precipitation is well represented. There are biases over the Plains, with too much precip-
337 itation west of the Mississippi river. This bias is probably due to diurnal cycle firing too
338 early and a dearth of propagating convective systems (see below). The Upper midwest
339 (Dakotas, Iowa, Minnesota) is too dry (and warm, see below) in summer. This is likely
340 due to a bias in clouds, which are also too low. The values indicate the percent root mean
341 square difference (PRMSD) between each simulation and ERA-Interim. The differences are 54%
342 for ne120 (uniform high resolution), 46% for ne30 (uniform low resolution) and 30% for
343 the variable mesh.

344 Why is CAM6 α variable resolution sometimes 'better' than uniform high resolution?
345 As noted above, the low resolution (ne30) and VR simulations are slightly better tuned
346 globally than the high resolution simulation, and this affects the overall climate metrics.
347 Since the majority of the variable-resolution grid is at the same resolution as the low
348 resolution (ne30) simulation, the global mean climatologies should be closely matched

349 in the absence of significant physical parameterization resolution sensitivities [*Zarzycki*
350 *et al.*, 2015]. This also offers further support that the variable-resolution CESM frame-
351 work is dynamically consistent across scales when compared to globally-uniform resolution
352 counterparts, particularly with the CAM6 α configuration used here.

353 Figure 9 illustrates climatological precipitation anomalies for winter (December-
354 February) relative to ERAI. The variable mesh in most respects looks like the ne120
355 simulation over land, with significant reductions in bias near the edges of the domain
356 in the Pacific Northwest U.S, Texas and the Upper Mid-west. Winter (DJF) differences
357 from ERAI are significantly reduced in the Western U.S. due to better representation of
358 mountain ranges. DJF values of the PRMSD are 17% (ne120), 20% (ne30) and 19% (VR).

359 Figure 10 illustrates summer (JJA) surface temperature (Ts) biases relative to ERAI.
360 For all simulations, there is a 2–4°C positive bias in the Central U.S. in summer. This is a
361 known bias in many models [*Ma et al.*, 2014]. The Root Mean Square Difference is 2.6°C
362 for ne120, 2.1°C for ne30 but only 1.8°C for VR. The bias is due to a lack of cloud and
363 less shortwave cloud radiative cooling in summer. Ts bases are higher in ne120, because
364 of less cloud and less SW cloud radative effect. Biases are confined to the upper midwest
365 region, and are consistent with the dry bias to precipitation in this region (Figure 8) and
366 may be coupled to the precipitation bias through land surface (soil moisture) feedbacks.
367 The VR simulation does not reproduce the same midwest anomalies as uniform ne120, but
368 has smaller anomalies, more similar to uniform ne30. This might be because of different
369 large scale forcing outside the region of refinement (lower climate biases in variable mesh
370 and uniform ne30 than ne120). Winter (DJF) Ts biases (not shown) are generally <2-3°.

371 The model is slightly cooler over the northern Rockies with a warm anomaly in Nebraska,
372 Kansas.

373 One of the major goals of high resolution climate simulations is to represent the fre-
374 quency of extreme events with high fidelity. To assess this, we look at statistics of high fre-
375 quency (3 hourly averages) summertime (JJA) temperature and precipitation. Frequency
376 statistics are calculated on the native grid of each simulation. Since we are looking at
377 frequency distributions, the exact grid for each data set is not important (the metric is
378 frequency). For comparison to observations, it is difficult to find similar high frequency
379 statistics. We use gridded CPC daily precipitation analyses (25km, 0.25° resolution)
380 for comparison (reference) and also North American Regional Reanalyses (NARR) for 3
381 hourly statistics. We note in particular that NARR analyses represent another model at
382 ~ 32 km.

383 Figure 11 illustrates frequency distributions of precipitation. The VR simulation looks
384 similar to the high resolution intensities, and has higher extreme precipitation frequency
385 than the low resolution simulation, as expected. In winter (DJF, Figure 11 left panel), the
386 frequency only extends to 200mm day⁻¹ and the variable mesh and high resolution are
387 close to the CPC observations. Frequencies in summer go higher, and the variable mesh
388 and high resolution simulations have higher frequency of extreme precipitation (>300mm
389 day⁻¹). However, comparisons between gridded precipitation observations and high res-
390 olution reanalysis may not be exact. Extreme precipitation frequency (>400 mm day⁻¹)
391 may be too high in the high resolution simulations relative to CPC precipitation analyses.
392 The VR simulation is actually closer to observed even in the high resolution region.

393 Perhaps the more focused question is whether the variable resolution simulation repro-
394 duces the extremes seen in the high resolution simulation at the finest scales. Figure 12
395 shows frequencies for 3 hourly average precipitation on the native grid of the simulations
396 and the NARR reanalysis. Here high and variable resolution simulations are producing
397 the same statistics, all the way up to very infrequent and extreme precipitation values.
398 The similarity indicates the variable mesh is successful at reproducing the statistics from
399 the high resolution simulation. Extreme precipitation frequencies are much higher than
400 produced by NARR reanalyses. The extreme rain rates correspond to 150mm in 3 hours,
401 and are only sustained for 3 hours. It does not imply that the model precipitates 1.2m
402 at a grid point in a day, rather 0.15m in 3 hours. Note that NARR is at slightly lower
403 resolution, but produces extremes closer to ne30, which may not be correct (too low).

404 Another metric for looking at the extremes is to integrate the frequency over the ex-
405 tremes and ask what is the frequency of exceedance of a threshold value for temperature
406 or precipitation by integrating over the tail of the frequency distribution. This has the
407 advantage of also having enough statistics to be able to look at interannual variability
408 and changes in the exceedance frequency over time.

409 Figure 13 illustrates the frequency of exceedance of daily average summer (JJA) tem-
410 perature above 307K (34°C) from simulations. Because of the temperature bias in JJA of
411 ~ 2 K in the simulations, the frequency of exceedance above 305K (33 °C) is plotted for daily
412 averaged ERAI 2m-temperature. All 3 simulations have similar exceedance probabilities,
413 with the uniform high resolution about 0.2 (20%) higher. The variability from year to
414 year is only about 20% of the value ($\sigma \sim 0.015$). ERAI has about the same interannual
415 standard deviation ($\sigma = 0.012$), and the frequency of exceedance (when adjusted for the

416 model temperature bias) is similar to the VR simulation. There is also an increasing trend
417 in the frequency of extreme temperature in all the simulations (though not statistically
418 significant). This is consistent with changes in recent climate records indicating more
419 warm extremes [Meehl *et al.*, 2009]. Note that this is the only metric from the simulations
420 (or observations) that does show a trend, though not statistically significant.

421 Figure 14 shows exceedance probabilities for precipitation above 100 mm day⁻¹ for 3
422 hourly (A,C) and daily (B,D) time frequencies. The VR simulation (blue) generally does
423 a very good job of reproducing the high resolution simulation (red) for both 3 hourly
424 and daily frequencies (lower for daily). The low resolution simulation (green) does not
425 reproduce the frequency as well. In addition, the VR and high resolution simulations also
426 do a good job of reproducing the exceedance probability of daily precipitation relative to
427 the CPC gridded precipitation observations. Since extreme precipitation impacts are a
428 significant part of local and regional climate impacts, this is a significant achievement for
429 trying to simulate regional climate extremes. There is large interannual variability, and
430 no discernible trends.

431 Figure 15 illustrates the diurnal cycle of precipitation rates in June from the Tropical
432 Rainfall Measurement Mission (TRMM) satellite and model simulations. In Figure 15,
433 the color indicates the local time of peak precipitation, and the intensity of the color the
434 magnitude of the diurnal cycle. In June, satellite observations from TRMM illustrate that
435 the peak in precipitation is around 1500LT at the edge of the Rocky Mountains, and then
436 propagates later to the east, reaching the early morning near the Mississippi river. June
437 is the peak for these systems. Afternoon storms dominate the mid-west of Illinois through
438 Ohio, while a slightly earlier peak is seen from the Ozarks through the Appalachians, and

439 the S. E. US see a peak near 1500-1800LT. The oceans feature a morning peak in the Gulf
440 of Mexico and the Atlantic.

441 CAM simulations reproduce many of these features. This is new in CAM6 α : earlier
442 model versions had peaks in precipitation near noon LT, from a peak in convective precip-
443 itation [*Gervais et al.*, 2014]. The noon peak has been reduced in CAM6 α , with evening
444 peaks near the Rockies and in the Midwest. Propagating systems are not as evident, but
445 there are hints of the systems in Nebraska in the variable mesh simulations (Figure 15b).
446 The model reproduces the S.E. U.S. evening signal well. Notably, the intensities are
447 weaker in the simulations than TRMM, but the VR simulation seems to have slightly
448 more intense cycles, and a better representation of the upper plains from Colorado to
449 Montana. The overall fidelity is much better than in previous model versions.

4. Summary/Conclusions

450 In this paper, we have presented a hierarchy of simulations using the regionally-defined
451 SE dynamical core in CAM. VR configurations reproduce the statistics of a high resolution
452 run well in idealized baroclinic wave tests. This indicates that the variable-resolution mesh
453 is producing ‘correct’ dynamical flow solutions both inside and outside of the refined
454 region.

455 In mid-latitude aquaplanet tests, the CAM physical parameterizations do have sensitiv-
456 ity to resolution. CAM4 has a big difference between high and low resolutions, and inside
457 and outside of a mid-latitude refined mesh on an aquaplanet. CAM5 and CAM5-CLUBB
458 have more similar performance inside and outside of a refined mesh region, particularly
459 for cloud radiative effects. This indicates that newer versions of the physical parameteri-
460 zations (CAM5 and CAM5-CLUBB) are less sensitive to space and time scale resolution.

461 In aquaplanet tests in the tropics, the CAM5-CLUBB configuration produces more sim-
462 ilar precipitation amounts inside and outside of the refined mesh region in the tropics,
463 much better than CAM4 or CAM5 without CLUBB (Figure 4). There is still some com-
464 pensation between large scale and convective precipitation with CAM5-CLUBB, and this
465 can be seen in the temperature and humidity tendency terms in aquaplanet simulations.
466 But because CAM5-CLUBB has one less parameterization producing precipitation (no
467 separate shallow convective scheme), there is less compensation between schemes.

468 The compensation is a feature of the CAM physical parameterization suite. Large
469 scale condensation is an instantaneous process that removes all liquid supersaturation
470 whenever large scale condensation, CLUBB and the prognostic cloud microphysics are
471 run. In contrast, the convective parameterization has a timescale: it consumes instability
472 and produces mass flux and precipitation at a defined rate. As the time step changes, the
473 deep convective parameterization does less, and the large scale condensation (including
474 CLUBB and MG cloud microphysics) does more. This is a key feature of the model that
475 has to be considered. Smaller grid boxes produce larger vertical velocities and hence
476 more stratiform rain, that then reduces the moisture available for convection, which has
477 a timescale.

478 Variable mesh simulations can be an important tool for testing physical parameteriza-
479 tions across scales. The dynamics are stable, and the high resolution regions resemble
480 uniform high resolution in a baroclinic test case. In aquaplanet experiments for mid-
481 latitude storm tracks, broad scale measures of climate statistics (total cloud cover and
482 longwave cloud radiative effect) are stable in both CAM5 and CAM-CLUBB. Cloud forc-
483 ing inside and outside of refined regions in CAM-CLUBB is stable to within 0.2 Wm^{-2} .

484 In tropical experiments, all configurations with a common deep convection scheme have
485 decreased convective precipitation in the refined (high-resolution) region. The stratiform
486 precipitation is increased in the high resolution region. However, in CAM-CLUBB, the
487 balance of the two produces more similar total precipitation inside and outside of a refined
488 mesh region in the convergence on the equator: better than either CAM4 or CAM5. The
489 total heating and moistening tendencies in the near equatorial region are nearly the same
490 inside and outside of the refined mesh region in CAM-CLUBB, more so than CAM5 or
491 CAM4.

492 Finally, we have conducted detailed simulations with full physics and a refined mesh
493 over the continental United States (CONUS) with CAM5-CLUBB. We use a smaller
494 timestep appropriate to the finest resolution for the simulations, and do limited tuning.
495 Results indicate that for most metrics, the VR simulation reproduces high-resolution high
496 frequency statistics for temperature, precipitation and clouds in the CONUS region. This
497 is clear for example in winter orographic precipitation in the western US. In addition, the
498 model performs well against observations, including observations of extreme precipitation
499 frequency. Some local precipitation values are high, and there remains a positive bias in
500 summertime surface temperature, that is coupled to biases in clouds and precipitation.
501 Some of the bias patterns in VR simulations resemble the lower resolution mesh, which
502 may indicate that they result also from large scale forcing outside of the refined region.

503 By some metrics, the VR simulations have smaller biases than uniform high resolution
504 simulations. This is possible because the mean VR global climate tends to be dominated
505 by the low resolution region. The CAM6 α physics is optimized (tuned) for this low

506 resolution, thus there still likely is some minor scale sensitivity (although much less than
507 CAM4).

508 Overall, at all stages from idealized tests to aquaplanet to full physics, we have tested
509 CAM variable-resolution simulations against uniform high resolution meshes (the ‘ref-
510 erence’ case). We find that CAM5 and CAM5-CLUBB provides better stability across
511 resolutions than CAM4. The variable mesh CAM6 α version used here (Bogenschutz et al.
512 2017, submitted to JAMES) can accurately reproduce the climate statistics of the high
513 resolution mesh in the high resolution region. The variable resolution mesh also repro-
514 duces observed features of extreme precipitation, and all simulations produce a trend in
515 extreme temperatures in summer, but no trends in extreme precipitation over the period
516 1980 to 2005.

517 Global climate metrics carry through into the high resolution region. Global biases
518 in low resolution (ne30) and variable mesh are lower than the high resolution (ne120)
519 simulation, and this can result in lower biases in the high resolution region. Indicating
520 that the high resolution region does feel the global climate metrics, and adjustments to
521 match observations. VR simulations may have distinct advantages for climate simulation
522 over uniform high resolution if the model is better optimized (tuned) for lower resolution.

523 Thus, the variable resolution framework with physics that is stable across resolutions can
524 accurately reproduce regional climate statistics of a high resolution simulation. CAM6 α
525 with the spectral element dynamical core is such a model. This does not require nesting,
526 or forcing multiple models, and is thus an energetically consistent approach for efficient
527 high resolution regional climate simulation.

528 **Acknowledgments.** The National Center for Atmospheric Research is Sponsored by
529 the U. S. National Science Foundation. Computer Resources provided by CHAP and ASD
530 awards. This work was supported at NCAR by a U.S. National Science Foundation (NSF)
531 grant for a Climate Process Team (CPT) on cloud-aerosol interactions (AGS-0968640), A
532 NSF Earth System Modeling (EaSM) grant on multi-scale modeling (AGS-1049057) and
533 a U.S. Department of Energy SciDAC grant on Tropical Biases (DE-SC0006702). Model
534 output from the simulations (climatologies and summary statistics) are available upon
535 inquiry to the corresponding author. Model code will be released in CESM2.

536 .

References

- 537 Bacmeister, J. T., M. F. Wehner, R. B. Neale, A. Gettelman, C. Hannay, P. H. Lauritzen,
538 J. M. Caron, and J. E. Truesdale (2014), Exploratory High-Resolution Climate Simula-
539 tions using the Community Atmosphere Model (CAM), *J. Climate*, *27*(9), 3073–3099,
540 doi:10.1175/JCLI-D-13-00387.1.
- 541 Bacmeister, J. T., K. A. Reed, C. Hannay, P. Lawrence, S. Bates, J. E. Truesdale,
542 N. Rosenbloom, and M. Levy (2016), Projected changes in tropical cyclone activity un-
543 der future warming scenarios using a high-resolution climate model, *Climatic Change*,
544 pp. 1–14, doi:10.1007/s10584-016-1750-x.
- 545 Bogenschutz, P. A., S. K. Krueger, and M. Khairoutdinov (2010), Assumed Probability
546 Density Functions for Shallow and Deep Convection, *J. Adv. Model. Earth Syst.*, *2*(4),
547 10, doi:10.3894/JAMES.2010.2.10.

- 548 Bogenschutz, P. A., A. Gettelman, H. Morrison, V. E. Larson, C. Craig, and D. P.
549 Schanen (2013), Higher-order turbulence closure and its impact on Climate Simula-
550 tion in the Community Atmosphere Model, *Journal of Climate*, *26*(23), 9655–9676,
551 doi:10.1175/JCLI-D-13-00075.1.
- 552 Chen, M., W. Shi, P. Xie, V. B. S. Silva, V. E. Kousky, R. Wayne Higgins, and J. E.
553 Janowiak (2008), Assessing objective techniques for gauge-based analyses of global daily
554 precipitation, *J. Geophys. Res.*, *113*(D4), D04,110, doi:10.1029/2007JD009132.
- 555 Dee, D. P., S. M. Uppala, A. J. Simmons, P. Berrisford, P. Poli, S. Kobayashi, U. Andrae,
556 M. A. Balmaseda, G. Balsamo, P. Bauer, P. Bechtold, A. C. M. Beljaars, L. van de Berg,
557 J. Bidlot, N. Bormann, C. Delsol, R. Dragani, M. Fuentes, A. J. Geer, L. Haimberger,
558 S. B. Healy, H. Hersbach, E. V. Hólm, L. Isaksen, P. K\`rallberg, M. Köhler, M. Matri-
559 cardi, A. P. McNally, B. M. Monge-Sanz, J.-J. Morcrette, B.-K. Park, C. Peubey, P. de
560 Rosnay, C. Tavolato, J.-N. Thépaut, and F. Vitart (2011), The ERA-Interim reanalysis:
561 Configuration and performance of the data assimilation system, *Quarterly Journal of*
562 *the Royal Meteorological Society*, *137*(656), 553–597, doi:10.1002/qj.828.
- 563 Gent, P. R., G. Danabasoglu, L. J. Donner, M. M. Holland, E. C. Hunke, S. R. Jayne,
564 D. M. Lawrence, R. B. Neale, P. J. Rasch, M. Vertenstein, P. H. Worley, Z.-L. Yang,
565 and M. Zhang (2011), The Community Climate System Model Version 4, *Journal of*
566 *Climate*, *24*(19), 4973–4991, doi:10.1175/2011JCLI4083.1.
- 567 Gervais, M., J. R. Gyakum, E. Atallah, L. B. Tremblay, and R. B. Neale (2014), How Well
568 Are the Distribution and Extreme Values of Daily Precipitation over North America
569 Represented in the Community Climate System Model? A Comparison to Reanalysis,
570 Satellite, and Gridded Station Data, *J. Climate*, *27*(14), 5219–5239, doi:10.1175/JCLI-

- 571 D-13-00320.1.
- 572 Gettelman, A. (2015), Putting the clouds back in aerosol–cloud interactions, *Atmos.*
573 *Chem. Phys.*, *15*(21), 12,397–12,411, doi:10.5194/acp-15-12397-2015.
- 574 Gettelman, A., and H. Morrison (2015), Advanced Two-Moment Bulk Microphysics for
575 Global Models. Part I: Off-Line Tests and Comparison with Other Schemes, *J. Climate*,
576 *28*(3), 1268–1287, doi:10.1175/JCLI-D-14-00102.1.
- 577 Golaz, J.-C., V. E. Larson, and W. R. Cotton (2002), A PDF-Based Model for Boundary
578 Layer Clouds. Part II: Model Results, *J. Atmos. Sci.*, *59*, 3552–3571.
- 579 Hack, J. J. (1994), Parameterization of moist convection in the National Center for Atmo-
580 spheric Research community climate model (CCM2), *J. Geophys. Res.*, *99*(D3), 5551–
581 5568, doi:10.1029/93JD03478.
- 582 Harris, L. M., and S.-J. Lin (2013), A two-way nested global-regional dynamical core on
583 the cubed-sphere grid, *Monthly Weather Review*, *141*(1), 283–306.
- 584 Huang, X., A. M. Rhoades, P. A. Ullrich, and C. M. Zarzycki (2016), An evaluation of
585 the variable-resolution CESM for modeling California’s climate, *J. Adv. Model. Earth*
586 *Syst.*, *8*(1), 345–369, doi:10.1002/2015MS000559.
- 587 Hurrell, J. W., M. Holland, P. Gent, S. Ghan, J. E. Kay, P. Kushner, J.-F. Lamarque,
588 W. Large, D. Lawrence, K. Lindsay, and others (2013), The Community Earth System
589 Model: A framework for collaborative research., *Bull. Am. Meteorol. Soc.*, *94*(9), 1339–
590 1360, doi:10.1175/BAMS-D-12-00121.1.
- 591 Jablonowski, C., and D. L. Williamson (2006), A baroclinic instability test case for atmo-
592 spheric model dynamical cores, *Quarterly Journal of the Royal Meteorological Society*,
593 *132*, 2943–2975, doi:10.1256/qj.06.12.

- 594 Kummerow, C., W. Barnes, T. Kozu, J. Shiue, and J. Simpson (1998), The Tropical Rain-
595 fall Measuring Mission (TRMM) Sensor Package, *J. Atmos. Oceanic Technol.*, *15*(3),
596 809–817, doi:10.1175/1520-0426(1998)015;0809:TTRMMT;2.0.CO;2.
- 597 Laprise, R. (2008), Regional climate modelling, *Journal of Computational Physics*, *227*(7),
598 3641–3666, doi:10.1016/j.jcp.2006.10.024.
- 599 Larson, V. E., J.-C. Golaz, and W. R. Cotton (2002), Small-Scale and Mesoscale Variabil-
600 ity in Cloudy Boundary Layers: Joint Probability Density Functions, *J. Atmos. Sci.*,
601 *59*(24), 3519–3539, doi:10.1175/1520-0469(2002)059;3519:SSAMVI;2.0.CO;2.
- 602 Ma, H.-Y., S. Xie, S. A. Klein, K. D. Williams, J. S. Boyle, S. Bony, H. Douville, S. Fer-
603 mepin, B. Medeiros, S. Tyteca, M. Watanabe, and D. Williamson (2014), On the Cor-
604 respondence between Mean Forecast Errors and Climate Errors in CMIP5 Models, *J.*
605 *Climate*, *27*(4), 1781–1798, doi:10.1175/JCLI-D-13-00474.1.
- 606 McGregor, J. L. (1997), Regional climate modelling, *Meteorol. Atmos. Phys.*, *63*(1-2),
607 105–117, doi:10.1007/BF01025367.
- 608 Mearns, L. O., R. Arritt, S. Biner, M. S. Bukovsky, S. McGinnis, S. Sain, D. Caya,
609 J. Correia, D. Flory, W. Gutowski, E. S. Takle, R. Jones, R. Leung, W. Moufouma-Okia,
610 L. McDaniel, A. M. B. Nunes, Y. Qian, J. Roads, L. Sloan, and M. Snyder (2012), The
611 North American Regional Climate Change Assessment Program: Overview of Phase I
612 Results, *Bull. Amer. Meteor. Soc.*, *93*(9), 1337–1362, doi:10.1175/BAMS-D-11-00223.1.
- 613 Meehl, G. A., C. Tebaldi, G. Walton, D. Easterling, and L. McDaniel (2009), Relative
614 increase of record high maximum temperatures compared to record low minimum tem-
615 peratures in the U.S., *Geophys. Res. Lett.*, *36*(23), L23,701, doi:10.1029/2009GL040736.

- 616 Mesinger, F., G. DiMego, E. Kalnay, K. Mitchell, P. C. Shafran, W. Ebisuzaki, D. Jović,
617 J. Woollen, E. Rogers, E. H. Berbery, M. B. Ek, Y. Fan, R. Grumbine, W. Higgins,
618 H. Li, Y. Lin, G. Manikin, D. Parrish, and W. Shi (2006), North American Regional
619 Reanalysis, *Bull. Amer. Meteor. Soc.*, *87*(3), 343–360, doi:10.1175/BAMS-87-3-343.
- 620 Neale, R. B., J. H. Richter, and M. Jochum (2008), The Impact of Convection on
621 ENSO: From a Delayed Oscillator to a Series of Events, *J. Climate*, *21*, 5904–+, doi:
622 10.1175/2008JCLI2244.1.
- 623 Neale, R. B., C. C. Chen, A. Gettelman, P. H. Lauritzen, S. Park, D. L. Williamson, A. J.
624 Conley, R. Garcia, D. Kinnison, J. F. Lamarque, D. Marsh, M. Mills, A. K. Smith,
625 S. Tilmes, F. Vitt, P. Cameron-Smith, W. D. Collins, M. J. Iacono, R. C. Easter,
626 S. J. Ghan, X. Liu, P. J. Rasch, and M. A. Taylor (2010), Description of the NCAR
627 Community Atmosphere Model (CAM5.0), *Tech. Rep. NCAR/TN-486+STR*, National
628 Center for Atmospheric Research, Boulder, CO, USA.
- 629 Neale, R. B., J. Richter, S. Park, P. H. Lauritzen, S. J. Vavrus, P. J. Rasch, and M. Zhang
630 (2013), The Mean Climate of the Community Atmosphere Model (CAM4) in Forced
631 SST and Fully Coupled Experiments, *J. Climate*, *26*(14), 5150–5168, doi:10.1175/JCLI-
632 D-12-00236.1.
- 633 Park, S., and C. S. Bretherton (2009), The University of Washington shallow convec-
634 tion and moist turbulence schemes and their impact on climate simulations with the
635 Community Atmosphere Model., *J. Climate*, *22*, 3449–3469.
- 636 Rauscher, S. A., T. D. Ringler, W. C. Skamarock, and A. A. Mirin (2012), Exploring a
637 Global Multiresolution Modeling Approach Using Aquaplanet Simulations, *J. Climate*,
638 *26*(8), 2432–2452, doi:10.1175/JCLI-D-12-00154.1.

- 639 Rhoades, A. M., X. Huang, P. A. Ullrich, and C. M. Zarzycki (2016), Characterizing
640 Sierra Nevada Snowpack Using Variable-Resolution CESM, *J. Appl. Meteor. Climatol.*,
641 *55*(1), 173–196, doi:10.1175/JAMC-D-15-0156.1.
- 642 Ringler, T. D., D. Jacobsen, M. Gunzburger, L. Ju, M. Duda, and W. Skamarock (2011),
643 Exploring a Multiresolution Modeling Approach within the Shallow-Water Equations,
644 *Mon. Wea. Rev.*, *139*(11), 3348–3368, doi:10.1175/MWR-D-10-05049.1.
- 645 Sakaguchi, K., L. R. Leung, C. Zhao, Q. Yang, J. Lu, S. Hagos, S. A. Rauscher, L. Dong,
646 T. D. Ringler, and P. H. Lauritzen (2015), Exploring a multi-resolution approach using
647 AMIP simulations, *Journal of Climate*, doi:10.1175/JCLI-D-14-00729.1.
- 648 Small, R. J., J. Bacmeister, D. Bailey, A. Baker, S. Bishop, F. Bryan, J. Caron, J. Dennis,
649 P. Gent, H.-m. Hsu, M. Jochum, D. Lawrence, E. Muñoz, P. diNezio, T. Scheitlin,
650 R. Tomas, J. Tribbia, Y.-h. Tseng, and M. Vertenstein (2014), A new synoptic scale
651 resolving global climate simulation using the Community Earth System Model, *J. Adv.*
652 *Model. Earth Syst.*, *6*(4), 1065–1094, doi:10.1002/2014MS000363.
- 653 Taylor, K. E. (2001), Summarizing multiple aspects of model performance in a single
654 diagram, *J. Geophys. Res.*, *106*(D7), 7183–7192, doi:10.1029/2000JD900719.
- 655 Taylor, M. A. (2011), Conservation of Mass and Energy for the Moist Atmospheric Primi-
656 tive Equations on Unstructured Grids, in *Numerical Techniques for Global Atmospheric*
657 *Models*, edited by P. Lauritzen, C. Jablonowski, M. Taylor, and R. Nair, pp. 357–380,
658 Springer Berlin Heidelberg, doi:10.1007/978-3-642-11640-7-12.
- 659 Wehner, M. F., K. A. Reed, F. Li, Prabhat, J. Bacmeister, C.-T. Chen, C. Paciorek,
660 P. J. Gleckler, K. R. Sperber, W. D. Collins, A. Gettelman, and C. Jablonowski (2014),
661 The effect of horizontal resolution on simulation quality in the Community Atmospheric

- 662 Model, CAM5.1, *J. Adv. Model. Earth Syst.*, 6(4), 980–997, doi:10.1002/2013MS000276.
- 663 Williamson, D. L. (2008), Convergence of aqua-planet simulations with increasing resolu-
664 tion in the Community Atmospheric Model, Version3, *Tellus*, 60A, 848–862.
- 665 Wu, C., X. Liu, Z. Lin, A. M. Rhoades, P. A. Ullrich, C. M. Zarzycki, Z. Lu, and S. R.
666 Rahimi-Esfarjani (2017), Exploring a variable-resolution approach for simulating re-
667 gional climate in the Rocky Mountain region using the VR-CESM, *Journal of Geophys-
668 ical Research: Atmospheres*, doi:10.1002/2017JD027008.
- 669 Zarzycki, C. M., and C. Jablonowski (2014), A multidecadal simulation of Atlantic tropical
670 cyclones using a variable-resolution global atmospheric general circulation model, *Jour-
671 nal of Advances in Modeling Earth Systems*, 6(3), 805–828, doi:10.1002/2014MS000352.
- 672 Zarzycki, C. M., and C. Jablonowski (2015), Experimental Tropical Cyclone Forecasts
673 Using a Variable-Resolution Global Model, *Mon. Wea. Rev.*, 143(10), 4012–4037, doi:
674 10.1175/MWR-D-15-0159.1.
- 675 Zarzycki, C. M., M. N. Levy, C. Jablonowski, J. R. Overfelt, M. A. Taylor, and P. A.
676 Ullrich (2014a), Aquaplanet Experiments Using CAM’s Variable-Resolution Dynamical
677 Core, *Journal of Climate*, 27(14), 5481–5503, doi:10.1175/JCLI-D-14-00004.1.
- 678 Zarzycki, C. M., C. Jablonowski, and M. A. Taylor (2014b), Using Variable-Resolution
679 Meshes to Model Tropical Cyclones in the Community Atmosphere Model, *Monthly
680 Weather Review*, 142(3), 1221–1239, doi:10.1175/MWR-D-13-00179.1.
- 681 Zarzycki, C. M., C. Jablonowski, D. R. Thatcher, and M. A. Taylor (2015), Effects of Lo-
682 calized Grid Refinement on the General Circulation and Climatology in the Community
683 Atmosphere Model, *J. Climate*, 28(7), 2777–2803, doi:10.1175/JCLI-D-14-00599.1.

684 Zhang, G. J., and N. A. McFarlane (1995), Sensitivity of climate simulations to the param-
685 eterization of cumulus convection in the Canadian Climate Center general circulation
686 model, *Atmos. Ocean*, *33*, 407–446.

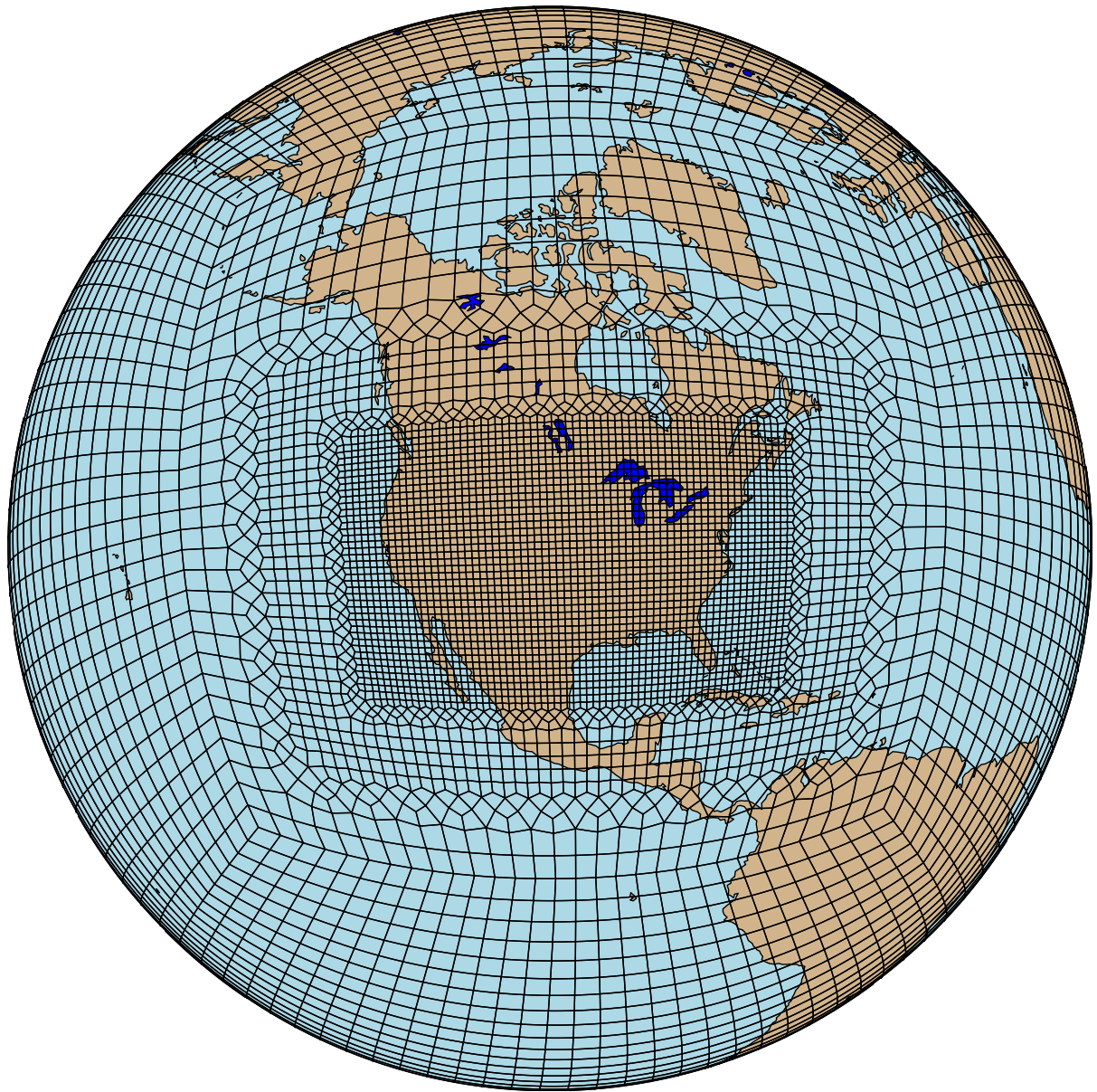


Figure 1. Continental United States (CONUS) variable resolution mesh for the Spectral Element (SE) dynamical core.

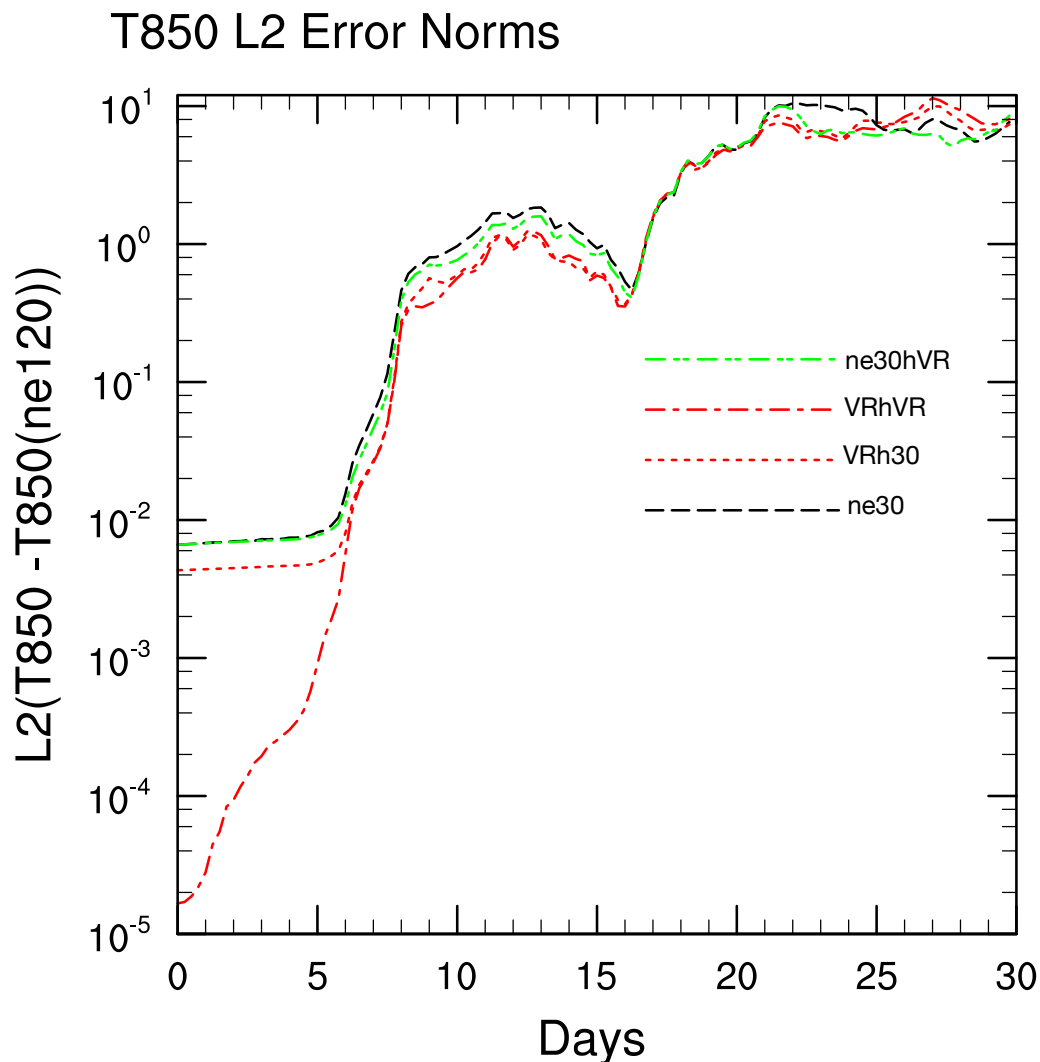


Figure 2. 850hPa temperature field L2 error norms following *Jablonowski and Williamson* [2006] inside a region of mid-latitude mesh refinement. L2 error norms show the difference from a reference, in this case uniform 0.25° (ne120) resolution, for variable mesh (VRhVR: red dot dash), variable mesh with unscaled ne30 hyperviscosity (VRh30: red dotted), uniform low resolution (ne30: black dash) and uniform low with with scaled hyperviscosity (ne30hVR: green dot-dash).

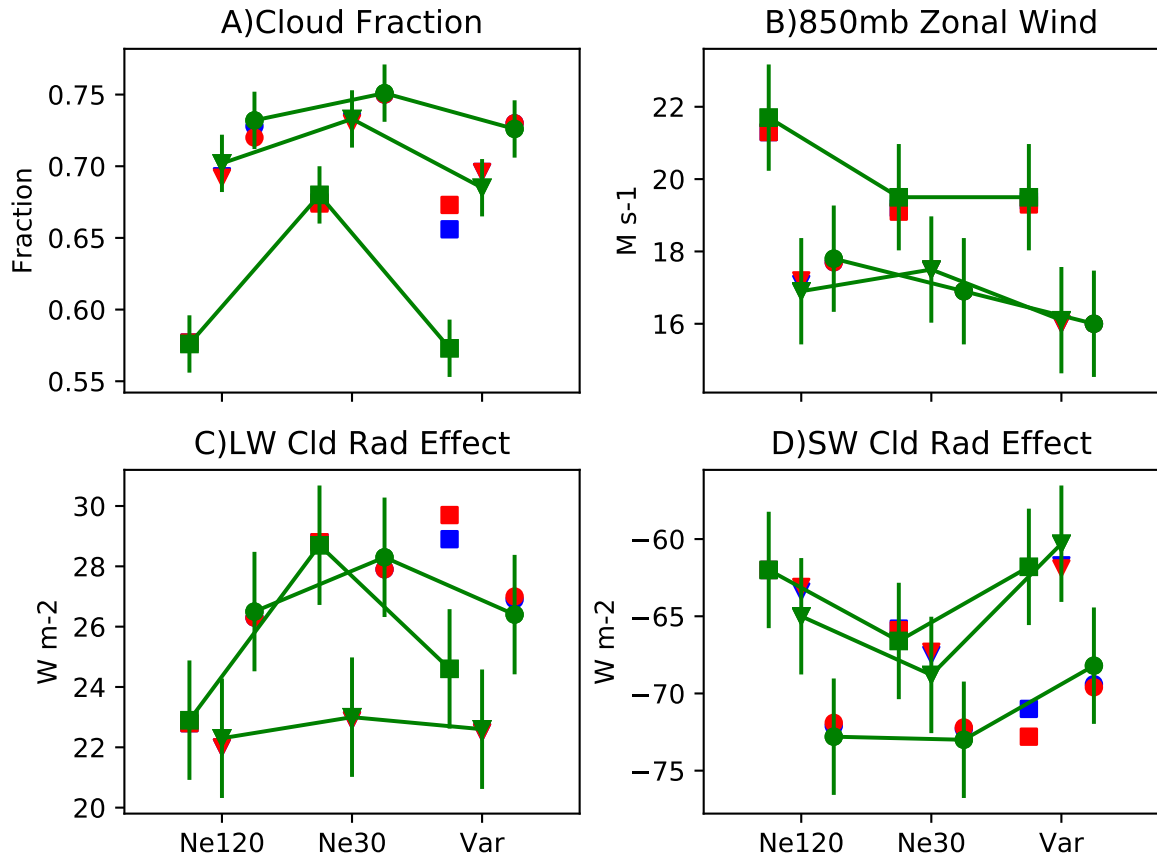


Figure 3. Mean 25°N–60°N statistics from Aquaplanet experiments. Zonal mean (Blue), inside the refined region (Green) and outside (Red). 9 different simulations are shown. 3 different resolutions shown as different x-axis positions: uniform 0.25° (ne120) resolution, uniform low (1°) resolution (ne30), variable mesh (Var) for each of 3 physics configurations: CAM4 (square), CAM5 (circle) and CAM-CLUBB (triangle). The lines connect the different values across resolutions for the refined region means. Error bars show one standard deviation of monthly means in the refined mesh region.

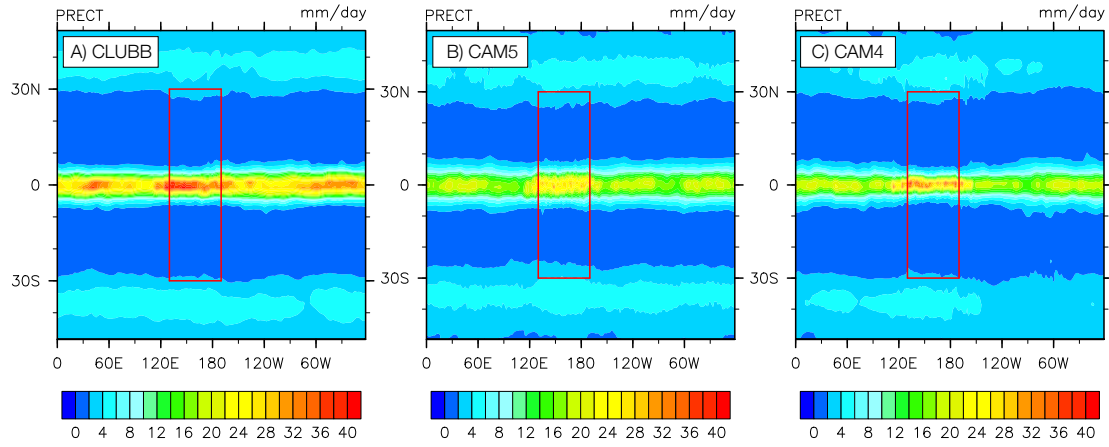


Figure 4. Total mean tropical precipitation rate (mm/day) from variable mesh aqua-planet simulations with different physics packages: CAM-CLUBB (left), CAM5 (center) and CAM4 (right)

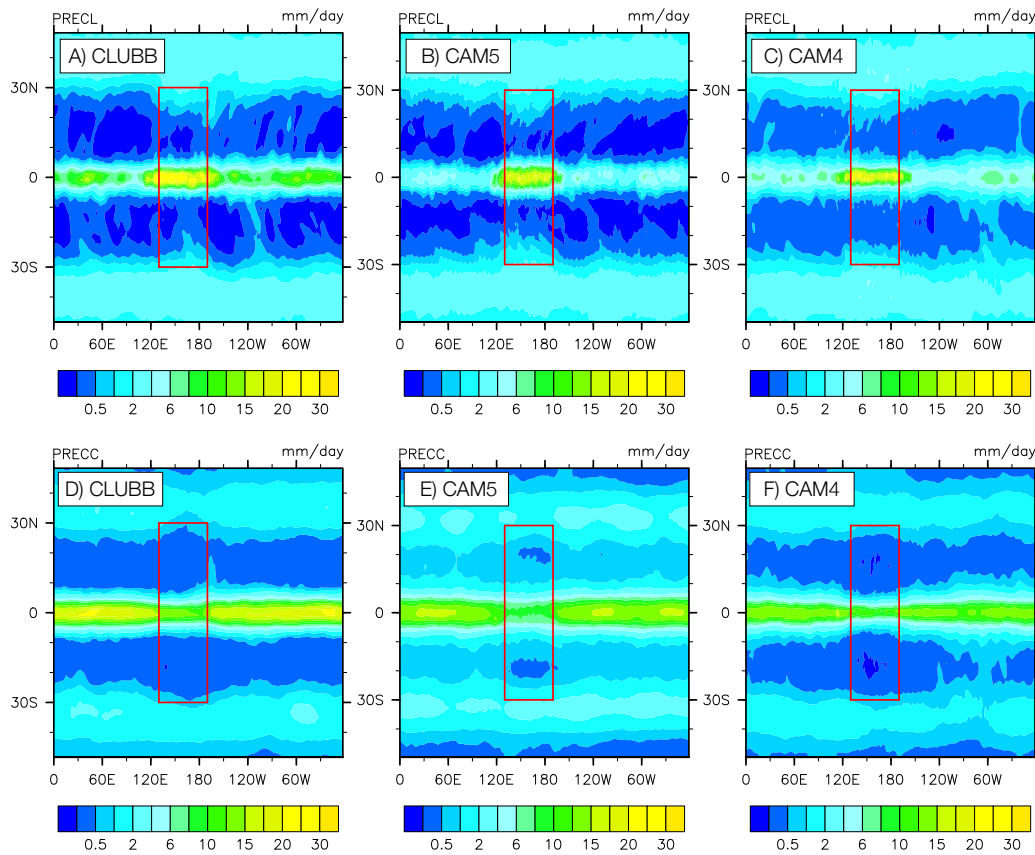


Figure 5. Tropical precipitation rates as in Figure 4 from variable mesh aquaplanet simulations. Top row: large scale precipitation, bottom row, convective precipitation.

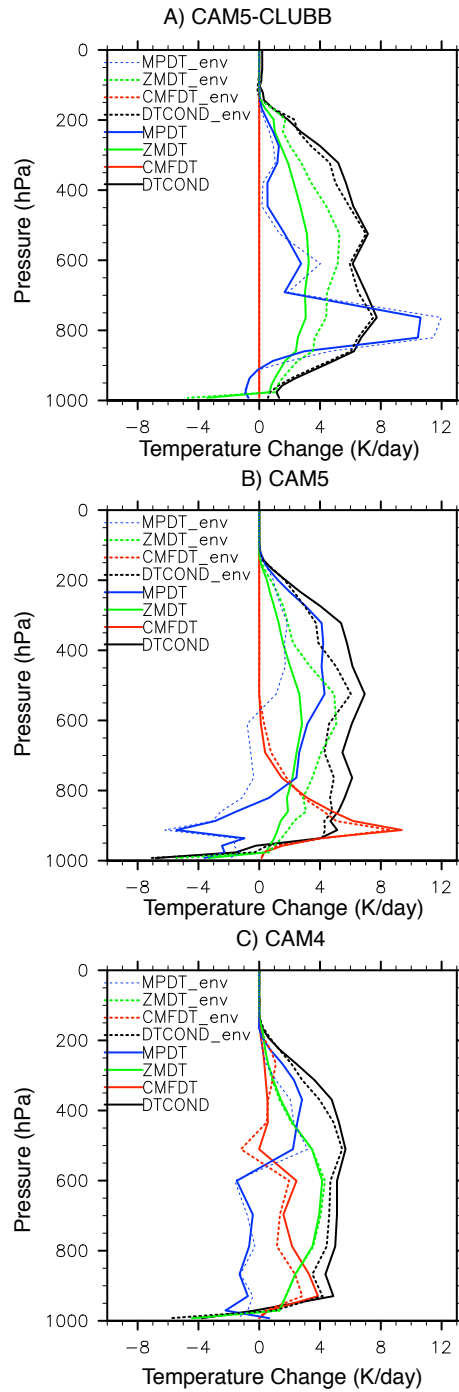


Figure 6. Temperature tendency profiles from (A) CAM-CLUBB, (B) CAM5 and (C) CAM4 averaged over 5S-5N and inside (solid) and outside (dashed) the region of refinement. The tendency terms are Deep convection (ZMDT: green), Shallow Convection (CMFDT: red), Large scale (macro and micro: MPDT blue), and Total (DTCOND: black).

D R A F T

November 1, 2017, 10:43pm

D R A F T

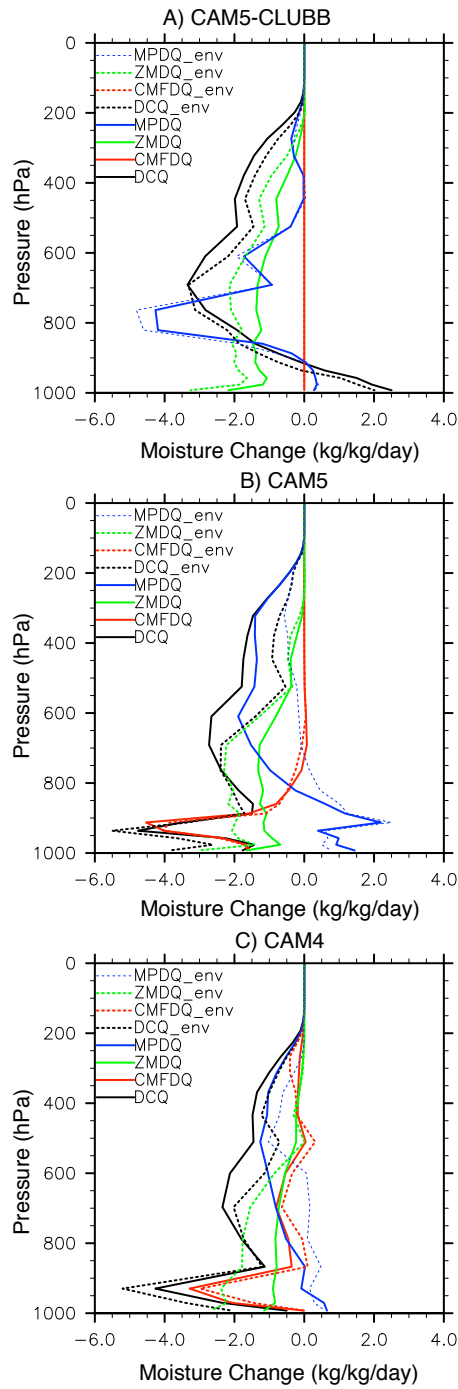


Figure 7. Humidity tendency profiles from (A) CAM-CLUBB, (B) CAM5 and (C) CAM4 averaged over 5S-5N and inside (solid) and outside (dashed) the region of refinement. The tendency terms are Deep convection (ZMDQ: green), Shallow Convection (CMFQ: red), Large scale (macro and micro: MPDQ blue), and DCQ Total (black).

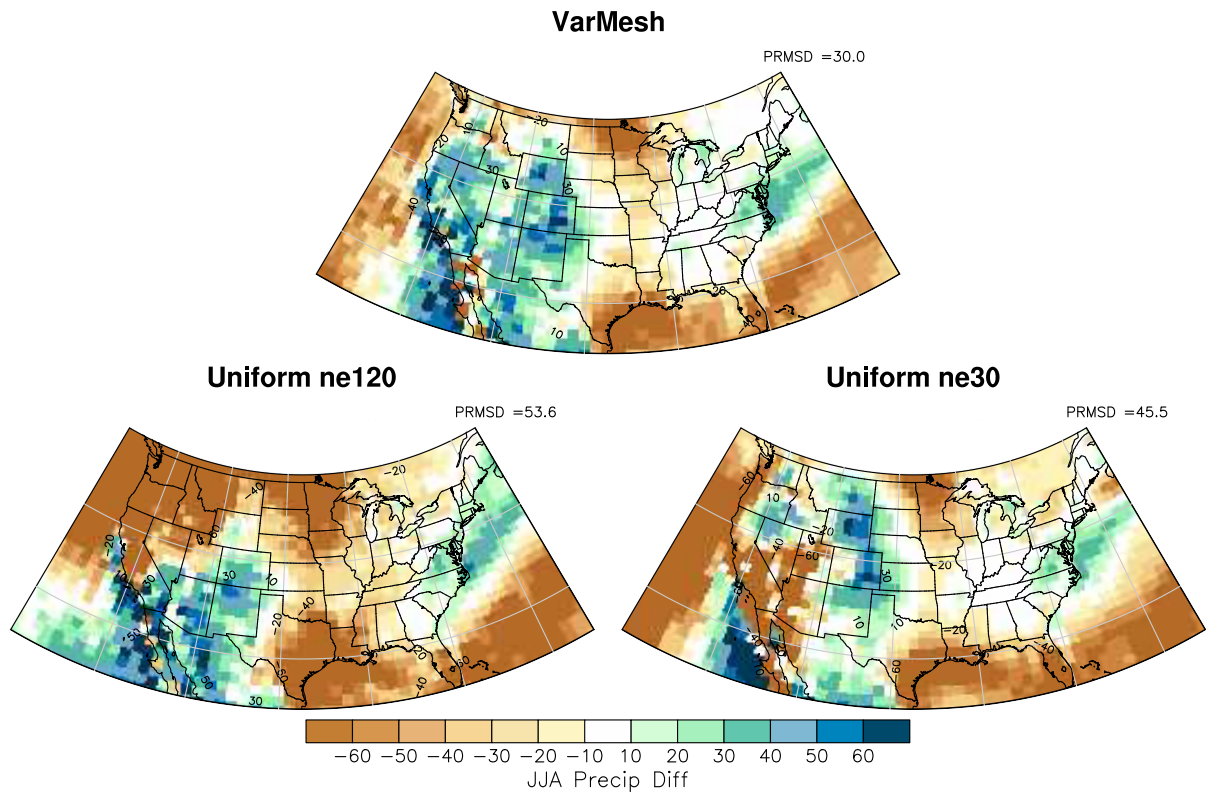


Figure 8. June-August percent difference between the CAM6 α CONUS simulations and ERAI climatological precipitation means. The values indicate the percent root mean square difference (PRMSD) between each simulation and ERAI.

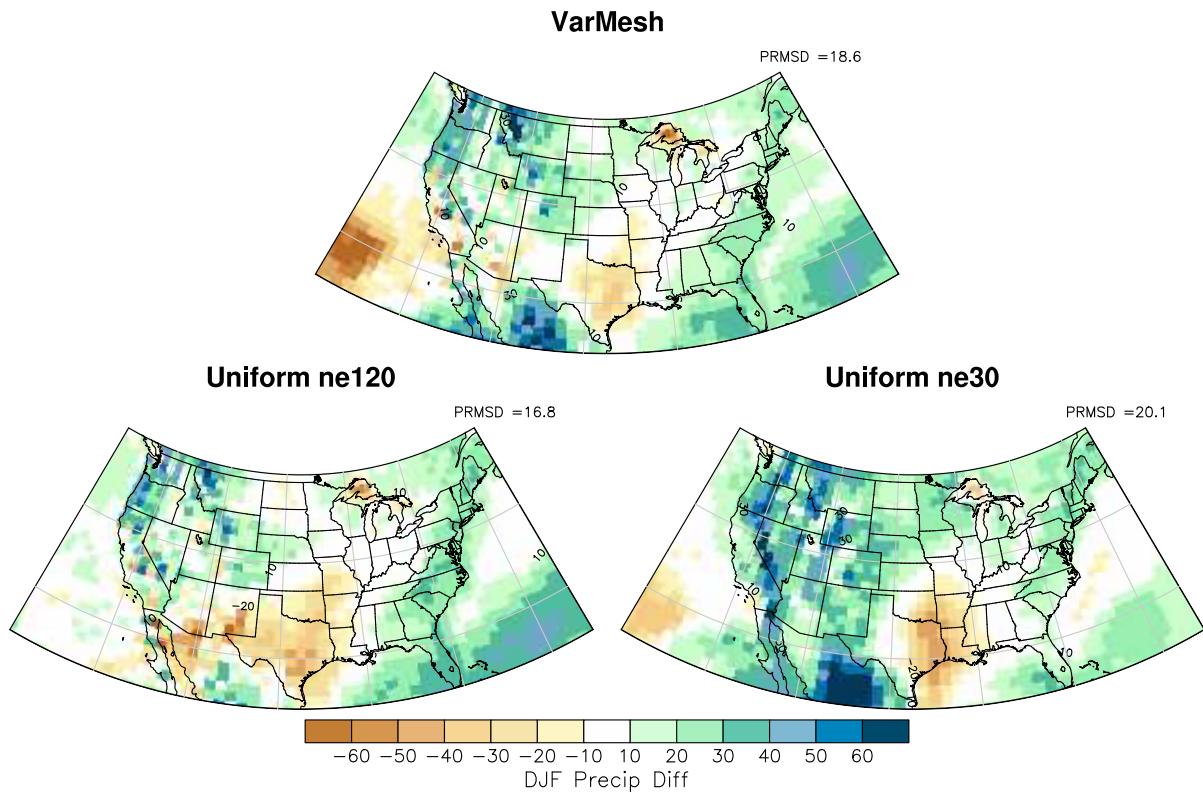


Figure 9. December-February percent difference between the CAM6 α CONUS simulations and ERAI climatological precipitation means. The values indicate the percent root mean square difference (PRMSD) between each simulation and ERAI.

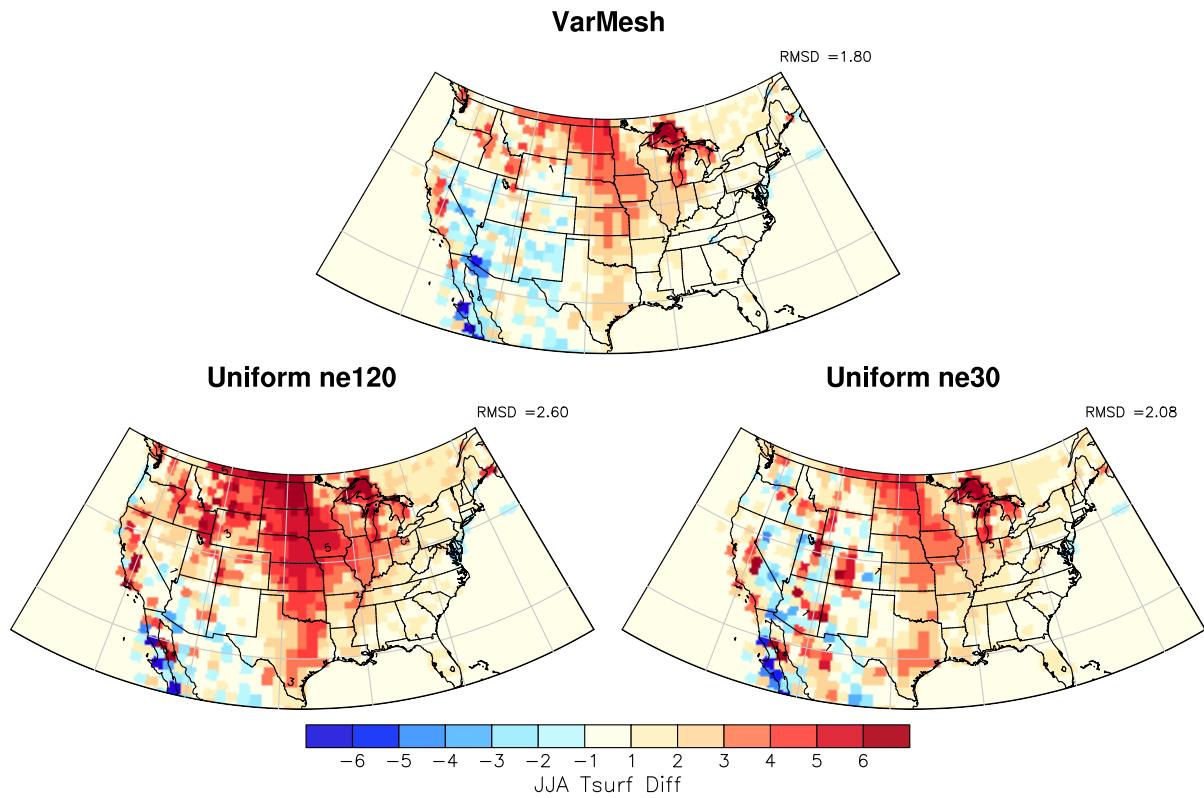


Figure 10. June-August difference between the CAM6 α CONUS simulations and ERAI climatological mean surface temperature. The values indicate the root mean square difference (RMSD) between each simulation and ERAI.

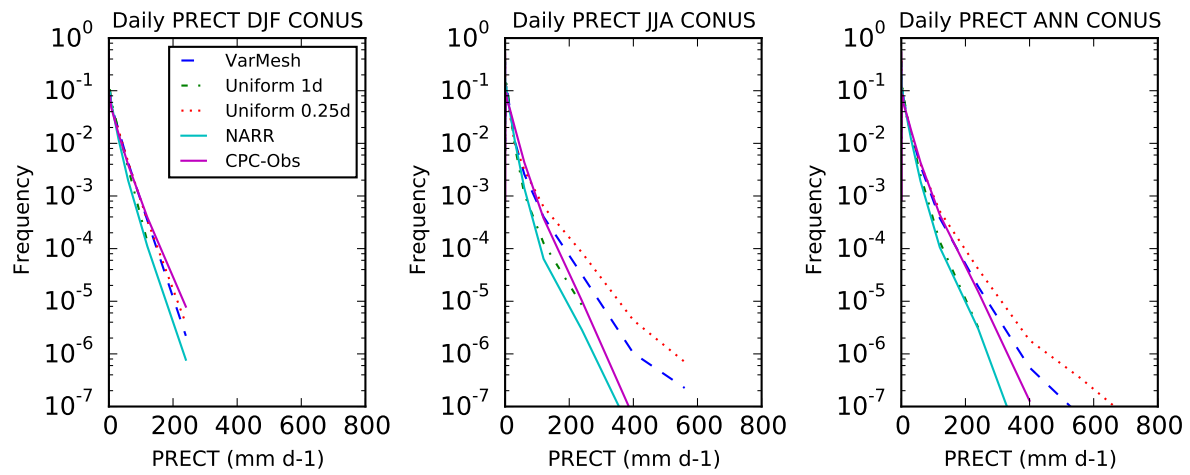


Figure 11. Daily Precipitation intensity histograms. Variable mesh (blue dash), Uniform high res (0.25° , red dot), Uniform low res (1° green dot dash) simulations and CPC observations (solid purple) and NARR reanalysis data (solid cyan).

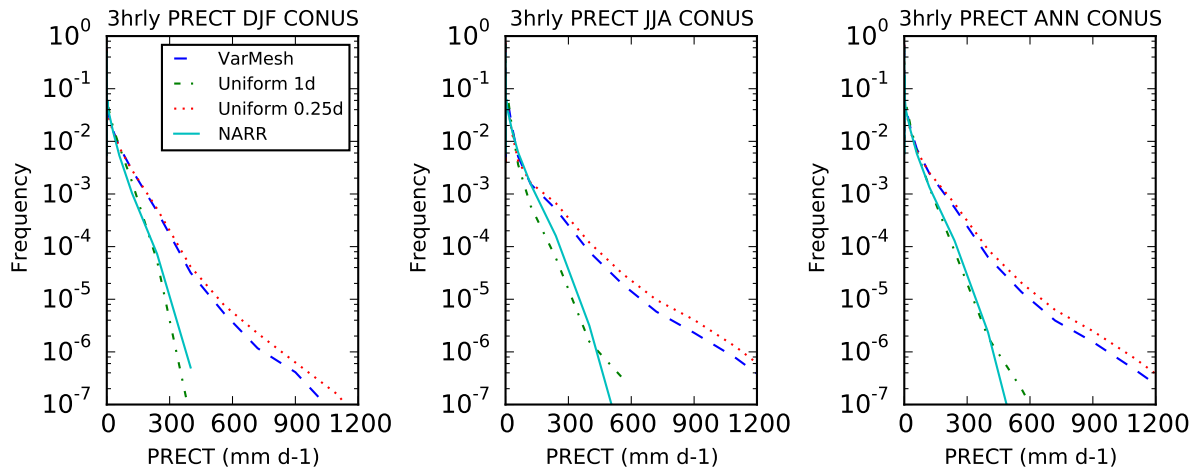


Figure 12. Precipitation intensity histograms from 3 hourly data (expressed in mm day⁻¹, but rates do not continue for a day). Variable mesh (blue dash), Uniform high res (0.25°, red dot), Uniform low res (1° cgreen dot dash) simulations and NARR reanalysis data (solid cyan).

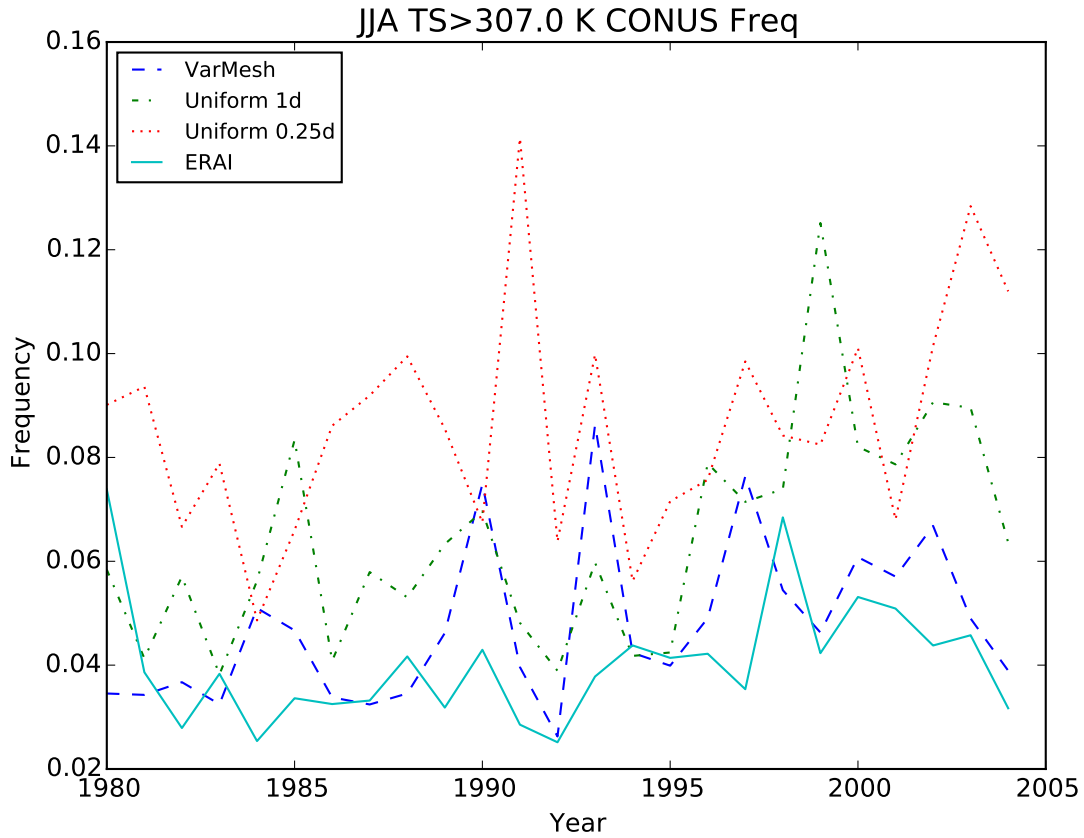


Figure 13. June-August (JJA) frequency of exceedance of daily average lowest level temperature above 307K (28°C). Variable mesh (blue dash), Uniform high res (0.25°, red dot), Uniform low res (1° green dot dash) simulations. Also shown is frequency of daily ERAI interim reanalysis data 2m temperature (solid cyan) above 305K.

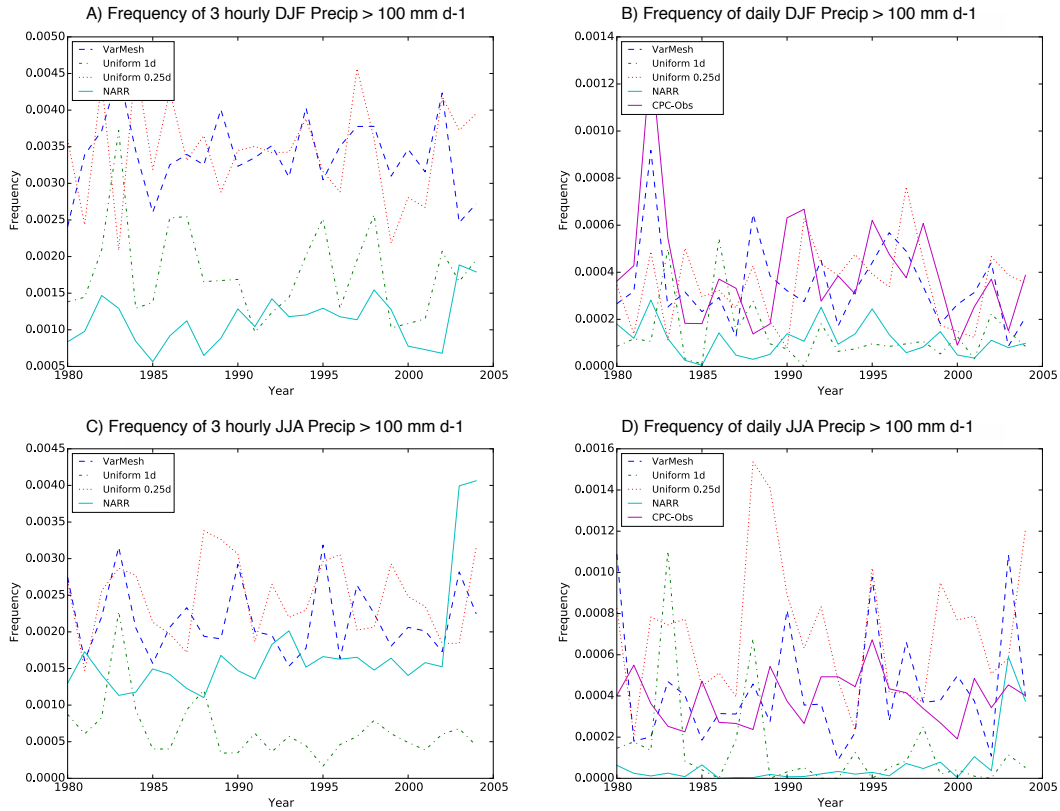


Figure 14. Frequency of exceedance of precipitation rates higher than 100mm day⁻¹ using (A,C) 3 hourly and (B,D) daily data for (A,B) December - February (DJF) and (C,D) June - August (JJA). Variable mesh (blue dash), Uniform high res (0.25°, red dot), Uniform low res (1° green dot dash) simulations, CPC observations (solid purple) and NARR reanalysis data (solid cyan).

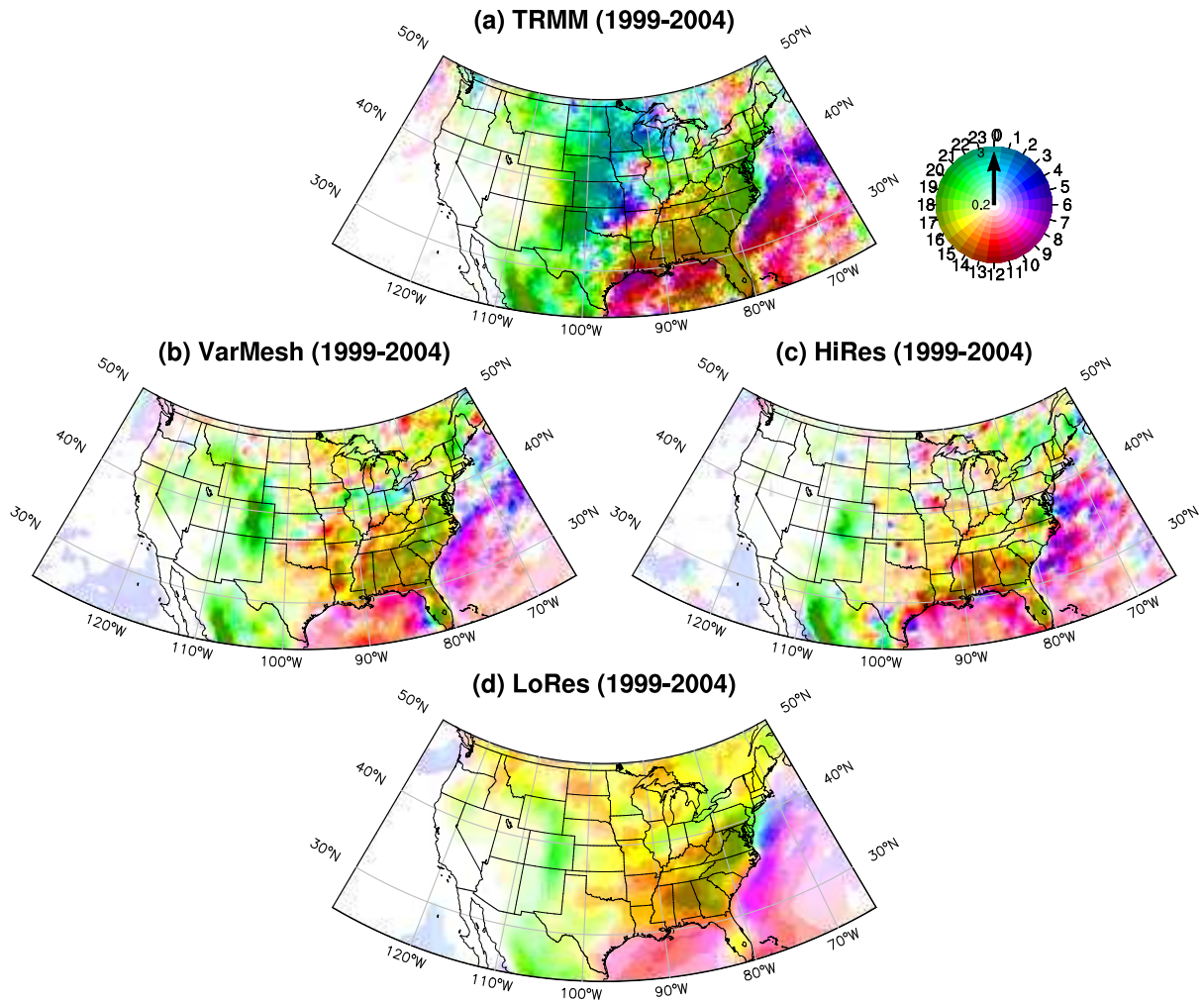


Figure 15. Diurnal cycle in June (6 year average from 1999-2004). (A) TRMM satellite observations, (B) Variable Mesh, (C) High Resolution (ne120), (D) Low Resolution (ne30). The local time peak of the diurnal cycle is shown in color on the color wheel. The intensity of the color is the amplitude.